Winter-Summer Contrast in the Response of Northern Hemisphere Precipitation Extremes to Climate Change

Andrew Williams[1] and Paul A. O'Gorman[2]

[1]Atmospheric, Oceanic and Planetary Physics, Department of Physics, University of Oxford, Oxford, UK,
[2]Department of Earth, Atmospheric and Planetary Sciences, Massachusetts Institute of Technology, Cambridge, MA, USA

Key Points:

- Over Northern Hemisphere land, models predict the fractional increase of precipitation extremes with warming is weaker in summer than winter
- The winter-summer contrast is primarily driven by weakened extreme ascent in summer due to decreases in near-surface relative humidity
- The winter-summer contrast is also evident in gridded observations of daily precipitation extremes, consistent with trends in CMIP5 models

Corresponding author: Andrew Williams, `andrew.williams@physics.ox.ac.uk`

Abstract

Climate models predict a distinct seasonality to future changes in daily extreme precipitation. In particular, models project that over land in the extratropical Northern Hemisphere the summer response is substantially weaker than the winter response in percentage terms. Here we decompose the projected response into thermodynamic and dynamic contributions and show that the seasonal contrast arises due to a negative dynamical contribution in northern summer due to weakened ascent, and a positive dynamical contribution and an anomalously strong thermodynamic contribution in northern winter. The negative dynamical contribution in northern summer is shown to relate to decreases in mean near-surface relative humidity with warming which suppress convection and associated upward motion in precipitation extremes. Finally, we show that the winter-summer contrast is also evident in observed trends of daily precipitation extremes in northern midlatitudes, which provides support for the contrast found in climate-model simulations.

1 Introduction

The impacts of extreme precipitation are felt acutely across the world with consequences ranging from floods and landslides (Kirschbaum et al., 2020) to changes in ecosystems (Knapp et al., 2008). Additionally, it is now well-understood that extreme precipitation events intensify overall on a global scale in response to global warming (Wehner et al., 2020; Kharin et al., 2013; O'Gorman, 2015). On regional scales however, the response of precipitation extremes to warming is uncertain, with some regions projected to experience changes in precipitation extremes which are much higher or lower than the global-mean intensification (Pfahl et al., 2017). Put together, this makes regional changes in extreme precipitation potentially one of the most impactful consequences of global warming and makes understanding historical and future changes in regional extreme precipitation important not only from a scientific perspective, but also for understanding the unequal impacts of climate change (Diffenbaugh & Burke, 2019). In addition, considering precipitation extremes in different seasons helps to clarify physical drivers and can also be important for impacts.

To understand projections of changes in precipitation extremes it is useful to decompose the changes into contributions from different physical drivers. One such approach is to use the simple, physical scaling developed by O'Gorman and Schneider (2009) which relates the intensity of precipitation extremes, P_e, to the pressure vertical velocity (ω_e) and the vertical derivative of saturation specific humidity with respect to pressure assuming a moist adiabatic lapse rate ($\frac{\mathrm{dq}_s}{\mathrm{dp}}|_{\theta^*}$),

$$P_e \sim -\left\{\omega_e \left.\frac{\mathrm{dq}_s}{\mathrm{dp}}\right|_{\theta^*}\right\}, \tag{1}$$

where $\{\cdot\}$ denotes a mass-weighted vertical integral over the troposphere, ω_e is evaluated on the day of the extreme event, and $\frac{\mathrm{dq}_s}{\mathrm{dp}}|_{\theta^*}$ is evaluated using the temperature T_e on the day of the extreme event. Thus, when considering a change in precipitation extremes due to global warming, δP_e, we can decompose the change into a thermodynamic contribution associated with changes in T_e and a dynamic contribution associated with changes in extreme ascent ω_e,

$$\delta P_e \;\approx\; \delta P_{\mathrm{therm}} \;+ \delta P_{\mathrm{dyn}}. \tag{2}$$

Pfahl et al. (2017) recently showed that Eq. 1 successfully captures the present-day pattern of Rx1day in the models and reanalysis and future changes in the models and thus is a good proxy for understanding and decomposing these future changes (Fig.

S1). They also used this scaling to decompose future regional changes in annual and seasonal maximum daily precipitation (hereafter, Rx1day) in simulations from the Coupled Model Intercomparison Project Phase 5, CMIP5, (Taylor et al., 2012) into thermodynamic and dynamic contributions. The thermodynamic contribution is positive and relatively spatially uniform, whereas the dynamic contribution varies strongly between regions and seasons and can either locally amplify or counteract the increases from the thermodynamic contribution.

The results of Pfahl et al. (2017) show a pronounced winter-summer contrast in the response of seasonal Rx1day. The fraction of land experiencing robust increases is relatively small in June-July-August (JJA), due to a negative dynamical contribution over land, particularly over Europe and North America. Similar results were found by Tandon et al. (2018) for the CanESM2 large ensemble. By contrast, Pfahl et al. (2017) found a relatively strong response of precipitation extremes in the Northern Hemisphere (NH) extratropics for December-January-February (DJF), and climate change was found to induce a shift in precipitation extremes towards the cold season in this region. Marelle et al. (2018) also found a shift towards the cold season for many regions in both CMIP5 models and regional models from the Coordinated Regional Downscaling Experiment (CORDEX). Furthermore, Marelle et al. (2018) found that the CMIP5 and CORDEX models could reproduce most aspects of the seasonality of precipitation extremes in the current climate when compared to gridded observations, which increases confidence in their future projections for changes in seasonality.

High-resolution, regional models have also shown a stronger response of precipitation extremes to climate change in DJF than JJA in Europe (Wood & Ludwig, 2020). This winter-summer contrast was also found in convection-permitting simulations of the Mediterranean (Pichelli et al., 2021) and the Contiguous United States (Prein et al., 2017), which is notable since convection-permitting simulations are better able to represent short-duration precipitation extremes (Prein et al., 2015). Precipitation extremes in JJA are known to be sensitive to how convection is represented (Chan et al., 2014; Prein et al., 2015; Ban et al., 2015; Kooperman et al., 2014) and caution is needed for projections in regions and seasons with significant mesoscale convective activity, particularly for sub-daily extremes. This emphasizes the importance of seeking observational evidence and robust physical mechanisms that may support projected seasonal changes in precipitation extremes.

Here, we focus on the winter-summer contrast in the fractional response of daily precipitation extremes to climate warming in the Northern Hemisphere in CMIP5 models and gridded observations. We begin by describing the model output and observational data and the methods of analysis (Section 2). We then show that the winter-summer contrast is primarily due to differences in the dynamical contribution between winter and summer, but that differences in the thermodynamic contribution also play a role, particularly at high latitudes (Section 3). We further show that the negative dynamical contribution in summer is strongly related in terms of model scatter and spatial pattern to decreases in mean near-surface relative humidity over land which inhibit convection (Section 4). Finally, we demonstrate that the winter-summer contrast is also evident in gridded observational datasets and coupled climate models over the historical period (Section 5), before giving our conclusions (Section 6).

2 Methods

We analyse changes over 1950–2100 under the historical and RCP8.5 scenarios for CMIP5. All models are used that provide the required data. The scaling and decomposition based on Eq. 1 is taken from Pfahl et al. (2017), and further details can be found there, but we repeat the key points of the scaling analysis here. We do not use CMIP6 output because the scaling analysis was already done for CMIP5 and because there is little improvement in the simulation of daily precipitation extremes between CMIP5 and CMIP6 (Wehner et al., 2020).

Daily surface precipitation was used to calculate the maximum daily precipitation amount (Rx1day) for DJF and JJA in each year. Daily mean temperature and vertical pressure velocity on all available pressure levels at the location and day of each daily-maximum precipitation event (T_e and ω_e) were then used to calculate the full extreme precipitation scaling following Eq. 1 by performing a vertical integral over all tropospheric levels with ascent ($\omega_e < 0$). To calculate the thermodynamic contribution, this analysis is repeated but with ω_e replaced with its average over all years from 1950-2100.

To calculate the sensitivity to climate change, we first normalize Rx1day and the full and thermodynamic scalings by dividing by their average over the historical period (1950-2000). We then calculate the dynamic contribution as the difference between the full and thermodynamic scaling. This approach to calculating the dynamic contribution differs slightly from Pfahl et al. (2017), but yields similar results (e.g., compare our Fig. 1c with their Fig. S7d). We then regress these normalized time series against global- and annual-mean surface temperature anomalies over 1950-2000 using the Theil-Sen estimator to produce sensitivities in units of (% K^{-1}). This regression approach has been shown to provide more robust results compared to taking differences in multi-decadal means (Fischer et al., 2014). When presenting results for the seasonal contrast (DJF-JJA), the sensitivities are calculated by differencing the normalized DJF and JJA time series in each grid box, before regressing this 'difference' time series against global-mean surface temperature anomalies for each model. Using a normalization over a reference period can sometimes produce statistical biases for changes in precipitation extremes (Donat et al., 2016; Sippel et al., 2017), but our results remain largely unchanged when using the full 1950-2100 period for normalization (Fig. S2).

All analysis is performed on each model's native grid, and then the sensitivities are re-gridded to a uniform 1°x1° grid before calculating multi-model statistics and zonal means. Pfahl et al. (2017) noted previously that some models produce very low seasonal Rx1day at some grid points in the subtropics, which creates anomalously large extreme precipitation sensitivities. Thus, when calculating multi-model or zonal means we exclude grid boxes from models where the average seasonal Rx1day over the historical period is less than 0.5 mm day^{-1}. Additionally, we found that the CMCC-CMS model produced unrealistically large changes in the thermodynamic component over Pakistan and Afghanistan, and so for this model we exclude the region from 29.5° to 32.5° latitude and 60° to 68° longitude.

We also analyse changes in seasonal Rx1day over the historical period over land in observations and compare them to the same period in the CMIP5 simulations (combining the historical and RCP8.5 simulations). We analyse the 'extended' NH winter (NDJFM) and summer (MJJAS) seasons (as opposed to DJF and JJA) to improve the signal-to-noise ratio and use data from 1950-2017, with the time-period chosen for maximum overlap with the CMIP5 data. For Rx1day observations, we focus on the HadEX3 gridded dataset (Dunn et al., 2020) which has a spatial resolution of 1.25° x 1.875°, but we also show results for the GHCNDEX observational dataset (Donat et al., 2013) which has a resolution of 2.5° x 2.5° in the supplement as a point of comparison. To calculate annual- and global-mean surface temperatures (including land and ocean) from observations, we use the NOAA Merged Land-Ocean Surface Temperature Analysis (Vose et al., 2012).

Sensitivities in % K^{-1} for the observations are calculated at each gridbox as described earlier but requiring at least 45 years of data at that grid box and normalizing by an average over all the years used. When analysing the winter-summer contrast (here, NDJFM-MJJAS) we require each grid box to have 45 years of data for both seasons in each year, and we normalize each time series separately before differencing and then performing the regression. CMIP5 data are subsampled to the observations in both space and time. To reduce the influence of unforced variability and outliers, we then aggregate the sensitivities into 5° latitude bands and calculate the median sensitivity across each latitude band. We use bootstrapping to estimate the uncertainty due to inter-annual variability and the non-uniform spatial coverage of the observations. To do this we calculate 10,000 bootstrap samples per latitude band, where each sample involves a random choice of both the years used in each grid box to calculate the regression, and a random choice of the grid boxes used to calculate the median sensitivity across the latitude band. We then calculate the median sensitivity for each bootstrap sample, and then the 90% confidence interval across samples for each latitude band. Our conclusions are largely insensitive to the size of the latitude bands and the number of bootstrap samples used, except in the tropics where larger latitude bands can obscure seasonal migrations of the ITCZ.

3 Winter-Summer contrast in CMIP5

Figure 1 shows the multi-model mean patterns of seasonal Rx1day sensitivity based on the scaling Eq. 1 and its decomposition into thermodynamic and dynamic components for DJF, JJA and DJF-JJA. As found in previous studies, the thermodynamic component is relatively uniform with robust agreement on the sign and the magnitude in both seasons. In stark contrast, the dynamic component exhibits strong regional and seasonal variations.

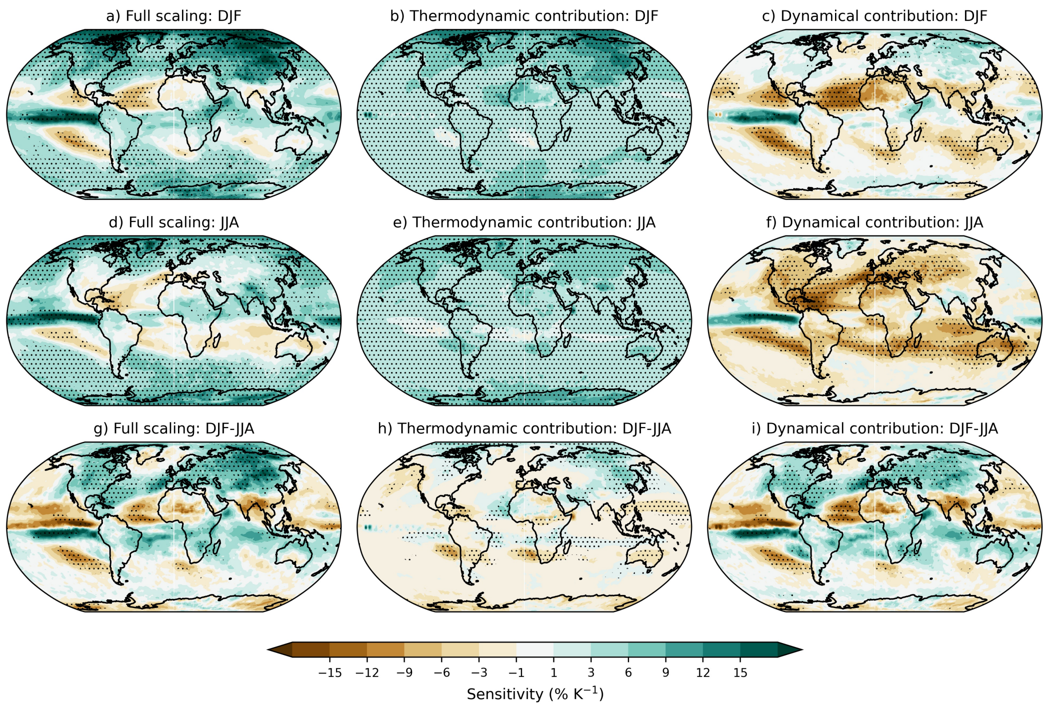

Figure 1. Multi-model mean Rx1day sensitivity over 1950-2100 according to the scaling Eq. 1 (a,d,g) and decomposition into (b,e,h) thermodynamic and (c,f,i) dynamic components for (a-c) DJF, (d-f) JJA and (e-i) DJF minus JJA, the winter-summer contrast. Stippling indicates where at least 90% of the models agree on the sign of the change.

The NH extratropics show a strongly positive DJF-JJA contrast especially over land (Fig. 1g). Over this region, the DJF response (Fig. 1a) is amplified by a positive contribution from the dynamics (Fig. 1c) and a relatively strong thermodynamic contribution particularly at high latitudes (Fig. 1b). On the other hand, the response during JJA is 'muted', with much less multi-model agreement and with some regions (particularly Europe and the continental United States) exhibiting close to no change or even negative responses of extreme precipitation to warming (Fig. 1d). This weak JJA response arises predominantly due to the strongly negative dynamical component (Fig. 1f) which cancels out the robust, positive increase due to the thermodynamic component (Fig. 1e). The combination of the amplified response in DJF and the very weak response in JJA leads to the strong DJF-JJA difference in the response, particularly over NH midlatitude land. The dynamical contribution is responsible most of the DJF-JJA difference, as illustrated by the similarity between in Fig. 1g and i, but seasonal differences in the thermodynamic contribution also play a role (Fig. 1h).

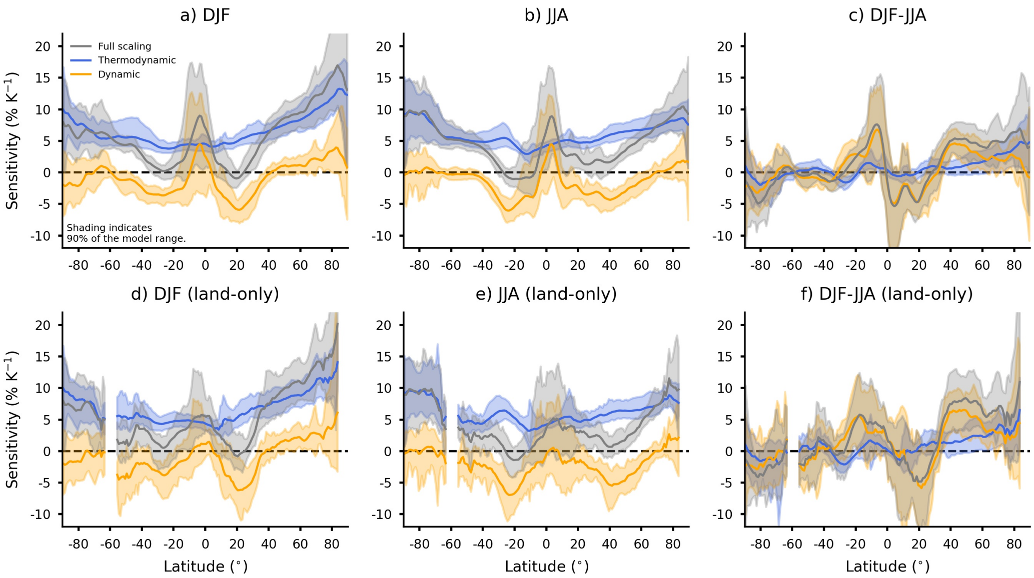

Figure 2. Zonal-means of the changes over 1950-2100 according to the scaling and its decomposition into thermodynamic and dynamic components for (a) DJF, (b) JJA and (c) DJF-JJA. Lines indicate multi-model means and shading shows the 90% model range. Panels (d,e,f) show the same results but for over land only.

Zonal-mean changes in the scaling decomposition are shown over both land and ocean and over land only (Fig. 2). The thermodynamic contribution is larger at higher latitudes (e.g., Fig. 2a,d) and is partly responsible for the DJF-JJA contrast at NH middle and high latitudes (Fig. 2c,f), implying a stronger thermodynamic contribution in winter than summer. A stronger thermodynamic contribution is expected for the lower temperatures in winter and at higher latitudes because percentage increases in $\frac{dq_s}{dp}|_{\theta^*}$ with increasing temperature are larger at lower temperatures (O'Gorman & Schneider, 2009). Arctic amplification of surface warming could also play a role, but the stronger thermodynamic contribution at higher (and colder) latitudes is also found to occur even when a globally uniform surface warming is imposed (O'Gorman et al., 2021).

In the tropics, the zonal-mean results in Fig. 2 are consistent with amplification of precipitation extremes along the ITCZ region, which moves seasonally. This leads to a southward shift in precipitation extremes when considering the seasonal contrast (Fig.

2c,f) because the ITCZ occurs further south in DJF than in JJA. These shifts are driven by the dynamical component as demonstrated by the similarity between the changes in the full scaling and the dynamic contribution in the tropics (gray and orange lines in Fig. 2c,f).

We have presented results in terms of percentage changes in (% K^{-1}) as opposed to absolute changes (mm day^{-1} K^{-1}) because it is useful to consider the change in each season relative to what is expected for that season and because previous studies have also focused on percentage changes which are easier to relate to physical processes. Absolute changes also show a seasonal contrast for much of NH midlatitude land but not for some parts of Asia (Fig. S3g) or for zonal-mean quantities (Fig. S4f), because the thermodynamic contribution offsets the dynamical contribution when considering absolute changes. Thus, one additional advantage of considering percentage changes is that it provides a strong zonal-mean signal to look for in the observational record (Section 5).

4 Physical mechanism of the negative dynamical contribution in summer

Dynamical weakening of precipitation extremes during JJA is a large contributor to the DJF-JJA contrast in the extratropical NH particularly over land (Figs. 1f and 2e). Physically then, what mechanisms could be responsible for this dynamical weakening? Tandon et al. (2018) tackled this question using a three-term approximation of the QG-ω equation and found the weakening of extreme ascent was related to increases in the horizontal length scale of extreme ascent. However, Li and O'Gorman (2020) numerically inverted the QG-ω equation in extreme precipitation events and found that changes in eddy length were less important when all terms were retained in the QG-ω equation, although they did not separately analyse extremes in JJA.

Here we investigate an alternative, simpler explanation in terms of changes in the near-surface relative humidity ($\mathrm{RH_{2m}}$). Decreases in $\mathrm{RH_{2m}}$ over land are expected with global-warming because of the land-ocean warming contrast (Byrne & O'Gorman, 2016, 2018) and decreases in stomatal conductance (Cao et al., 2010; Berg et al., 2016). Although relative humidity does not appear explicitly in Eq. 1, decreases in relative humidity can inhibit convection and the associated upward motion ω_e in precipitation extremes, implying a negative dynamical contribution under climate change. Previous work has already shown that decreases in relative humidity cause an increase in convective inhibition that is particularly large over NH land in JJA (Chen et al., 2020), and here we show this is linked to the dynamical contribution to changes in precipitation extremes.

In Fig. 3 we compare the sensitivities of seasonal-mean $\mathrm{RH_{2m}}$ and the dynamical component of precipitation extremes during JJA for climate change over 1950-2100. The sensitivity of $\mathrm{RH_{2m}}$ is defined using regression analogously to the sensitivity of precipitation extremes and normalized by the 1950-2000 mean. There is strong agreement between the spatial pattern of the change in $\mathrm{RH_{2m}}$ and the dynamical contribution (Fig. 3a,b), with the models agreeing robustly on strong decreases in relative humidity and a negative dynamical component over similar regions of the globe (see also Figs. S5 and S6 for individual models). Furthermore, Fig. 3c shows that models with a stronger decrease in JJA $\mathrm{RH_{2m}}$ also tend to have a stronger negative dynamical contribution when averaged over NH midlatitude land. In NH DJF, there is not a connection between changes in $\mathrm{RH_{2m}}$ and the dynamical contribution (Fig. S7), which we hypothesize is because wintertime daily precipitation extremes are controlled to a greater extent by large-scale dynamics as compared to the strongly convective extremes in summer.

The relationship between changes in mean relative humidity and the negative dynamical contribution to changes in extreme precipitation in JJA is notable in that it links changes in a mean quantity to changes in an extreme statistic. Such a link is potentially

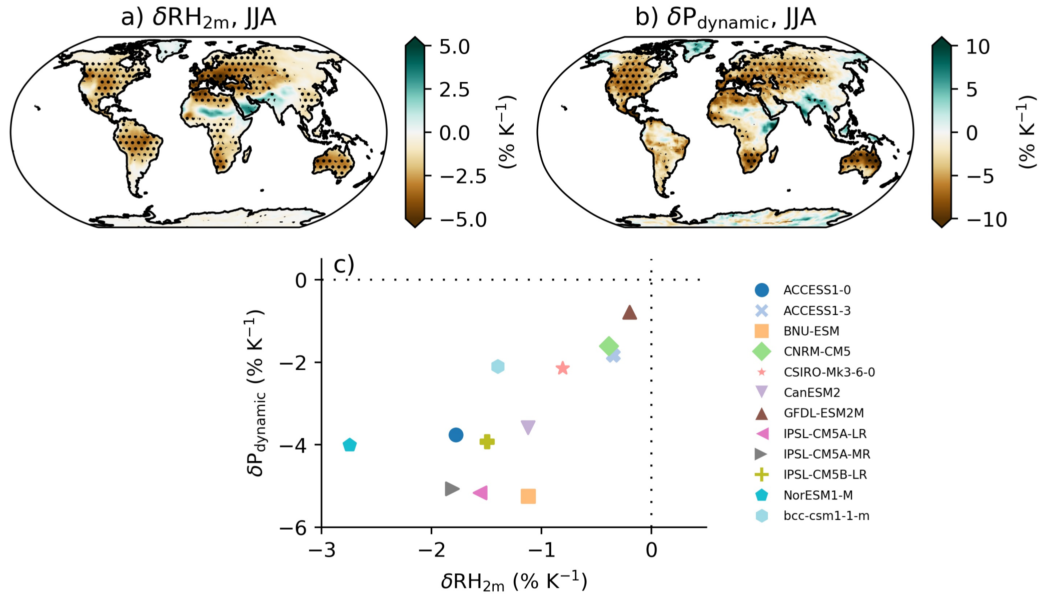

Figure 3. Sensitivity for JJA over 1950-2100 of (a) seasonal-mean near-surface relative humidity and (b) the dynamical contribution to changes in precipitation extremes. Results are shown for the 12 models that archived RH_{2m} and for which the dynamical component was calculated. Stippling indicates where 10 out the 12 models agree on the sign of the sensitivity. Panel (c) shows a scatter plot of the median sensitivities across land grid boxes in the latitude band 40-70°N for each model.

very useful since mean quantities can be easier to observationally constrain than extremes. The mechanism we propose is only valid over land where the negative dynamical contribution is strongest, and other factors such as a general weakening of the extratropical storm track in NH JJA (O'Gorman, 2010; Gertler & O'Gorman, 2019), poleward expansion of the Hadley cells (Pfahl et al., 2017), or other aspects of the large-scale dynamics (Tandon et al., 2018) may also play a role.

5 Observed and modelled trends over the historical period

Given the difficulty in correctly representing convection in models, we next turn our attention to gridded observations of precipitation extremes. Figure 4 shows the sensitivity of daily precipitation extremes from HadEX3 observations and CMIP5 models to warming over 1950-2017 for boreal extended winter (NDJFM) and summer (MJJAS), and the seasonal contrast (NDJFM-MJJAS). The results are expressed as medians over 5° latitude bands (see Methods). For the NH extratropics, the observed sensitivities are positive in both NDJFM and MJJAS, and there is a clear winter-summer contrast with higher sensitivities in NDJFM than MJJAS (Fig.4a,b,c). The seasonal contrast is also evident when looking at maps of the sensitivities, but as expected there is considerable noise when considering sensitivities for a period of this length in individual gridboxes (Fig.S8 a,b,c). The NH extratropical winter-summer contrast is also present in the CMIP5 models over the same historical period (Fig.4 d,e,f).

We next quantify the NH midlatitude response by averaging the sensitivities between 30-70°N with area-weighting. For the observations, the mean NH sensitivity is 11.6 % K^{-1} for NDJFM, 5.6 % K^{-1} for MJJAS, and 7.2 % K^{-1} for the winter-summer con-

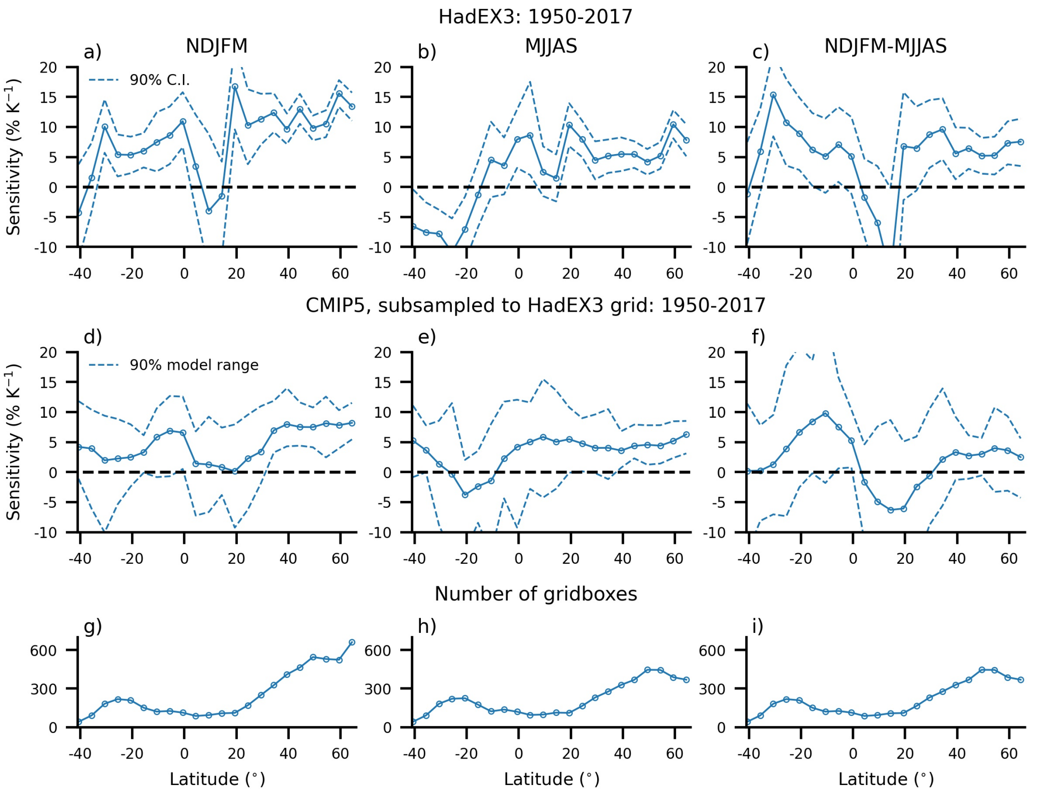

Figure 4. The sensitivity of Rx1day to warming over 1950-2017 in NDJFM (a,d), MJJAS (b,e) and DFJM-MJJAS (c,f) for the HadEX3 dataset (a,b,c) and CMIP5 simulations subsampled to the HadEX3 dataset (d,e,f). Solid lines show the median sensitivity across the 5° latitude band. Dashed lines show the 90% confidence interval for HadEX3 and 90% of the model spread for CMIP5. The total number of grid-boxes included in each latitude band is also shown (g,h,i) which is the same for both the observations and the simulations.

trast. For the CMIP5 models over the same period, the multimodel-mean sensitivity and full model range are 7.0 % K^{-1} (4.7 to 10.8 % K^{-1}) for NDJFM, 4.4% K^{-1} (2.1 to 9.1 % K^{-1}) for MJJAS, and 2.4 % K^{-1} (-0.6 to 8.4 % K^{-1}) for NDJFM-MJJAS. Thus, while the models and observations show similar sensitivities during NH summer, none of the models capture the very strong observed sensitivity for NH winter. As a result, while the observed winter-summer contrast lies within the model range, the multimodel-mean value is lower than the observations. Most but not all models (15/18) give a positive winter-summer contrast for this period consistent with the observations.

GHCNDEX has a coarser spatial resolution and fewer grid boxes with data compared to HadEX3, particularly in the tropics (Fig. S8), but we find similar changes in seasonal Rx1day over the Northern Hemisphere, which strengthens our confidence in the results (Figs. S8 and S9). Similar results are also found when the CMIP5 data are not subsampled to the observations (Figure S10), which suggests that missing grid points in the observations are not affecting our conclusions. The robust presence of the winter-summer contrast in observed trends over the historical period supports the contrast found in earlier sections.

6 Conclusions

In this study we have demonstrated that CMIP5 models project a robust seasonal contrast in the response of precipitation extremes to warming over the extratropical Northern Hemisphere, with considerably stronger percentage changes in winter than summer. We have also shown that this winter-summer contrast is evident in gridded observations over the historical period which strengthens our confidence in the future projections. CMIP5 simulations over the historical period also show a winter-summer contrast that occurs in 15/18 models, and the model range includes the observed value of this contrast.

Furthermore, we have used a simple, physical scaling to help explain the cause of the winter-summer contrast in changes in precipitation extremes. The contrast is primarily caused by the dynamical contribution (related to changes in extreme ascent) with a weakly positive dynamical contribution in DJF and a strongly negative dynamical contribution in JJA. The negative dynamical contribution in JJA is strongest over land, and we argue it is linked to strong decreases in near-surface relative humidity over land, which increase convective inhibition and impedes the associated upward motion in precipitation extremes. This mechanism is supported by a match between the spatial pattern and intermodel scatter of changes in relative humidity and the dynamical contribution.

The thermodynamic contribution to changes in precipitation extremes also helps to amplify the response in winter over summer, particularly over high latitudes and this is because the thermodynamic contribution is larger at lower temperatures when considering percentage changes. We have focused on percentage seasonal changes because they may be more relevant for impacts in a given season and to better connect with physical mechanisms. If absolute rather than percentage changes in precipitation extremes are considered, the thermodynamic contribution is larger in summer than winter, and this offsets the winter-summer contrast in the dynamic contribution, although the contrast is still evident over much of NH midlatitude land (Fig. S3).

Future work could build on our observational analysis by performing a formal detection and attribution analysis of the seasonal difference in trends of precipitation extremes. Future work could also build more understanding of the positive dynamical contribution in NH winter, and further investigate the link between changes in near-surface relative humidity and precipitation extremes using idealized experiments in convection-permitting models. Given the potential importance of decreases in relative humidity over land for convection and precipitation extremes, it would be helpful to develop an emergent constraint for the magnitude of the expected decrease, although this may be difficult to the extent that it depends both on the land-ocean warming contrast and CO_2 through physiological effects.

Acknowledgments

A.W. acknowledges funding from the Natural Environment Research Council, Oxford DTP, Award NE/S007474/1 and the Laidlaw Research and Leadership Programme. P.A.O'.G. acknowledges support from NSF awards AGS-1552195 and AGS-1749986.

We acknowledge the World Climate Research Programme's Working Group on Coupled Modelling, which is responsible for CMIP, and we thank the climate modeling groups for producing and making available their model output. We thank Stephan Pfahl for generously providing the CMIP5 scaling data used for this study. A.W. thanks Ziwei Li for helpful discussions and Makayla Haussler for moral support and input on the figures. Processed data supporting this study can be found at https://doi.org/10.5281/zenodo.5557105.

References

Ban, N., Schmidli, J., & Schär, C. (2015). Heavy precipitation in a changing climate: Does short-term summer precipitation increase faster? *Geophysical Research Letters*, *42*(4), 1165–1172. doi: 10.1002/2014GL062588

Berg, A., Findell, K., Lintner, B., Giannini, A., Seneviratne, S. I., van den Hurk, B., … Milly, P. C. D. (2016). Land–atmosphere feedbacks amplify aridity increase over land under global warming. *Nature Climate Change*, *6*(9), 869–874. doi: 10.1038/nclimate3029

Byrne, M. P., & O'Gorman, P. A. (2016). Understanding decreases in land relative humidity with global warming: Conceptual model and GCM simulations. *Journal of Climate*, *29*(24), 9045–9061. doi: 10.1175/JCLI-D-16-0351.1

Byrne, M. P., & O'Gorman, P. A. (2018). Trends in continental temperature and humidity directly linked to ocean warming. *Proceedings of the National Academy of Sciences*, *115*(19), 4863–4868. doi: 10.1073/pnas.1722312115

Cao, L., Bala, G., Caldeira, K., Nemani, R., & Ban-Weiss, G. (2010). Importance of carbon dioxide physiological forcing to future climate change. *Proceedings of the National Academy of Sciences*, *107*(21), 9513–9518. doi: 10.1073/pnas.0913000107

Chan, S. C., Kendon, E. J., Fowler, H. J., Blenkinsop, S., Roberts, N. M., & Ferro, C. A. T. (2014). The value of high-resolution met office regional climate models in the simulation of multihourly precipitation extremes. *Journal of Climate*, *27*(16), 6155–6174. doi: 10.1175/JCLI-D-13-00723.1

Diffenbaugh, N. S., & Burke, M. (2019). Global warming has increased global economic inequality. *Proceedings of the National Academy of Sciences*, *116*(20), 9808–9813. doi: 10.1073/pnas.1816020116

Donat, M. G., Alexander, L. V., Yang, H., Durre, I., Vose, R., Dunn, R. J. H., … Kitching, S. (2013). Updated analyses of temperature and precipitation extreme indices since the beginning of the twentieth century: The HadEX2 dataset. *Journal of Geophysical Research: Atmospheres*, *118*(5), 2098–2118. doi: 10.1002/jgrd.50150

Donat, M. G., Lowry, A. L., Alexander, L. V., O'Gorman, P. A., & Maher, N. (2016). More extreme precipitation in the world's dry and wet regions. *Nature Climate Change*, *6*(5), 508–513. doi: 10.1038/nclimate2941

Dunn, R. J. H., Alexander, L. V., Donat, M. G., Zhang, X., Bador, M., Herold, N., … Bin Hj Yussof, M. N. (2020). Development of an updated global land in situ-based data set of temperature and precipitation extremes: HadEX3. *Journal of Geophysical Research: Atmospheres*, *125*(16), e2019JD032263. doi: 10.1029/2019JD032263

Fischer, E. M., Sedláček, J., Hawkins, E., & Knutti, R. (2014). Models agree on forced response pattern of precipitation and temperature extremes. *Geophysical Research Letters*, *41*(23), 8554–8562. doi: 10.1002/2014GL062018

Gertler, C. G., & O'Gorman, P. A. (2019). Changing available energy for extratropical cyclones and associated convection in northern hemisphere summer. *Proceedings of the National Academy of Sciences*, *116*(10), 4105–4110. doi: 10.1073/pnas.1812312116

Kharin, V. V., Zwiers, F. W., Zhang, X., & Wehner, M. (2013). Changes in temperature and precipitation extremes in the CMIP5 ensemble. *Climatic Change*, *119*(2), 345–357. doi: 10.1007/s10584-013-0705-8

Kirschbaum, D., Kapnick, S. B., Stanley, T., & Pascale, S. (2020). Changes in extreme precipitation and landslides over high mountain asia. *Geophysical Research Letters*, *47*(4), e2019GL085347. doi: 10.1029/2019GL085347

Knapp, A. K., Beier, C., Briske, D. D., Classen, A. T., Luo, Y., Reichstein, M., … Weng, E. (2008). Consequences of more extreme precipitation regimes for terrestrial ecosystems. *BioScience*, *58*(9), 811–821.

Kooperman, G. J., Pritchard, M. S., & Somerville, R. C. J. (2014). The response of US summer rainfall to quadrupled CO2 climate change in conventional and superparameterized versions of the NCAR community atmosphere model. *Journal of Advances in Modeling Earth Systems*, *6*(3), 859–882. doi: 10.1002/2014MS000306

Li, Z., & O'Gorman, P. A. (2020). Response of vertical velocities in extratropical precipitation extremes to climate change. *Journal of Climate*, *33*(16), 7125–7139. doi: 10.1175/JCLI-D-19-0766.1

Marelle, L., Myhre, G., Hodnebrog, , Sillmann, J., & Samset, B. H. (2018). The changing seasonality of extreme daily precipitation. *Geophysical Research Letters*, *45*(20), 11,352–11,360. doi: 10.1029/2018GL079567

O'Gorman, P. A., & Schneider, T. (2009). The physical basis for increases in precipitation extremes in simulations of 21st-century climate change. *Proceedings of the National Academy of Sciences*, *106*(35), 14773–14777. doi: 10.1073/pnas.0907610106

O'Gorman, P. A. (2010). Understanding the varied response of the extratropical storm tracks to climate change. *Proceedings of the National Academy of Sciences*, *107*(45), 19176–19180. doi: 10.1073/pnas.1011547107

O'Gorman, P. A. (2015). Precipitation extremes under climate change. *Current Climate Change Reports*, *1*(2), 49–59. doi: 10.1007/s40641-015-0009-3

O'Gorman, P. A., Li, Z., Boos, W. R., & Yuval, J. (2021). Response of extreme precipitation to uniform surface warming in quasi-global aquaplanet simulations at high resolution. *Philosophical Transactions of the Royal Society A: Mathematical, Physical and Engineering Sciences*, *379*(2195), 20190543. doi: 10.1098/rsta.2019.0543

Pfahl, S., O'Gorman, P. A., & Fischer, E. M. (2017). Understanding the regional pattern of projected future changes in extreme precipitation. *Nature Climate Change*, *7*(6), 423–427. doi: 10.1038/nclimate3287

Pichelli, E., Coppola, E., Sobolowski, S., Ban, N., Giorgi, F., Stocchi, P., … Vergara-Temprado, J. (2021). The first multi-model ensemble of regional climate simulations at kilometer-scale resolution part 2: historical and future simulations of precipitation. *Climate Dynamics*, *56*(11), 3581–3602. doi: 10.1007/s00382-021-05657-4

Prein, A. F., Langhans, W., Fosser, G., Ferrone, A., Ban, N., Goergen, K., … Leung, R. (2015). A review on regional convection-permitting climate modeling: Demonstrations, prospects, and challenges. *Reviews of Geophysics*, *53*(2), 323–361. doi: 10.1002/2014RG000475

Prein, A. F., Rasmussen, R. M., Ikeda, K., Liu, C., Clark, M. P., & Holland, G. J. (2017). The future intensification of hourly precipitation extremes. *Nature Climate Change*, *7*(1), 48–52. doi: 10.1038/nclimate3168

Sippel, S., Zscheischler, J., Heimann, M., Lange, H., Mahecha, M. D., van Oldenborgh, G. J., … Reichstein, M. (2017). Have precipitation extremes and annual totals been increasing in the world's dry regions over the last 60 years? *Hydrology and Earth System Sciences*, *21*(1), 441–458. doi: 10.5194/hess-21-441-2017

Tandon, N. F., Nie, J., & Zhang, X. (2018). Strong influence of eddy length on boreal summertime extreme precipitation projections. *Geophysical Research Letters*, *45*(19), 10,665–10,672. doi: 10.1029/2018GL079327

Taylor, K. E., Stouffer, R. J., & Meehl, G. A. (2012). An overview of CMIP5 and the experiment design. *Bulletin of the American Meteorological Society*, *93*(4), 485–498. doi: 10.1175/BAMS-D-11-00094.1

Vose, R. S., Arndt, D., Banzon, V. F., Easterling, D. R., Gleason, B., Huang, B., … Wuertz, D. B. (2012). NOAA's merged land–ocean surface temperature analysis. *Bulletin of the American Meteorological Society*, *93*(11), 1677–1685. doi: 10.1175/BAMS-D-11-00241.1

Wehner, M., Gleckler, P., & Lee, J. (2020). Characterization of long period return values of extreme daily temperature and precipitation in the CMIP6 models: Part 1, model evaluation. *Weather and Climate Extremes*, *30*, 100283. doi: 10.1016/j.wace.2020.100283

Wood, R. R., & Ludwig, R. (2020). Analyzing internal variability and forced response of subdaily and daily extreme precipitation over europe. *Geophysical Research Letters*, *47*(17), e2020GL089300. doi: 10.1029/2020GL089300